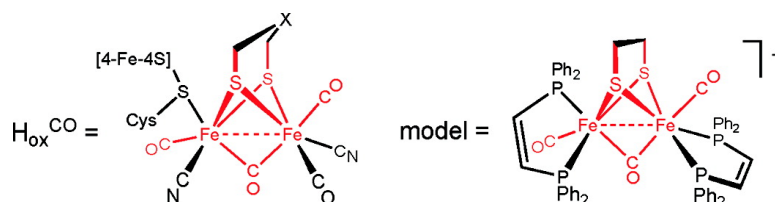Article

Diiron Dithiolato Carbonyls Related to the H State of [FeFe]-Hydrogenase

Aaron K. Justice, Mark J. Nilges, Thomas B. Rauchfuss,
Scott R. Wilson, Luca De Gioia, and Giuseppe Zampella

More About This Article

Additional resources and features associated with this article are available within the HTML version:

- Supporting Information
- Links to the 7 articles that cite this article, as of the time of this article download
- Access to high resolution figures
- Links to articles and content related to this article
- Copyright permission to reproduce figures and/or text from this article

View the Full Text HTML

ACS Publications
High quality. High impact.

Diiron Dithiolato Carbonyls Related to the H_{ox}^{CO} State of [FeFe]-Hydrogenase

Aaron K. Justice,[†] Mark J. Nilges,[†] Thomas B. Rauchfuss,*[,†] Scott R. Wilson,[†] Luca De Gioia,*[,‡] and Giuseppe Zampella[‡]

Department of Chemistry, University of Illinois at Urbana–Champaign, Urbana, Illinois 61801, and Department of Biotechnology and Biosciences, University of Milano−Bicocca, Piazza della Scienza 1, 20126 Milan, Italy

Received December 20, 2007; E-mail: rauchfuz@uiuc.edu

Abstract: Oxidation of the electron-rich ($E_{1/2} = -175$ vs Ag/AgCl) ethanedithiolato complex $Fe_2(S_2C_2H_4)(CO)_2(dppv)_2$ (**1**) under a CO atmosphere yielded $[Fe_2(S_2C_2H_4)(\mu\text{-}CO)(CO)_2(dppv)_2]^+$ ($[\mathbf{1}(CO)]^+$), a model for the H_{ox}^{CO} state of the [FeFe]-hydrogenases. This complex exists as two isomers: a kinetically favored unsymmetrical derivative, *unsym*-$[\mathbf{1}(CO)]^+$, and a thermodynamically favored isomer, *sym*-$[\mathbf{1}(CO)]^+$, wherein both diphosphines span apical and basal sites. Crystallographic characterization of *sym*-$[\mathbf{1}(CO)]^+$ confirmed a C_2-symmetric structure with a bridging CO ligand and an elongated Fe−Fe bond of 2.7012(14) Å, as predicted previously. Oxidation of *sym*-$[\mathbf{1}(CO)]^+$ and *unsym*-$[\mathbf{1}(CO)]^+$ again by $1e^-$ oxidation afforded the respective diamagnetic diferrous derivatives where the relative stabilities of the *sym* and *unsym* isomers are reversed. DFT calculations indicate that the stabilities of *sym* and *unsym* isomers are affected differently by the oxidation state of the diiron unit: the mutually trans CO ligands in the *sym* isomer are more destabilizing in the mixed-valence state than in the diferrous state. EPR analysis of mixed-valence complexes revealed that, for $[\mathbf{1}]^+$, the unpaired spin is localized on a single iron center, whereas for *unsym*/*sym*-$[\mathbf{1}(CO)]^+$, the unpaired spin was delocalized over both iron centers, as indicated by the magnitude of the hyperfine coupling to the phosphine ligands trans to the Fe−Fe vector. Oxidation of **1** by 2 equiv of acetylferrocenium afforded the dication $[\mathbf{1}]^{2+}$, which, on the basis of low-temperature IR spectrum, is structurally similar to $[\mathbf{1}]^+$. Treatment of $[\mathbf{1}]^{2+}$ with CO gives *unsym*-$[\mathbf{1}(CO)]^{2+}$.

Introduction

It is increasingly clear that both *in vitro* and *in silico* modeling efforts are crucial to developing a useful mechanistic understanding of the reactions catalyzed by the [FeFe]-hydrogenases. The spectroscopy of the enzymes themselves is complicated by the presence of multiple Fe−S clusters and the difficulties of observing reactive intermediates.[1,2] A key aspect of mechanistic modeling is, of course, the binding of substrates to the active site, although in the case of the hydrogenases, the only substrates, H_2 and H^+, are not readily observable. For this reason, there is considerable interest in the binding of the one known inhibitor, CO. Recent synthetic models for the H_{ox} state of the [FeFe]-hydrogenases are reactive toward CO,[3,4] which is known to bind to the apical site on the distal iron center of the active site (eq 1).[1,5,6]

$$\text{(1)}$$
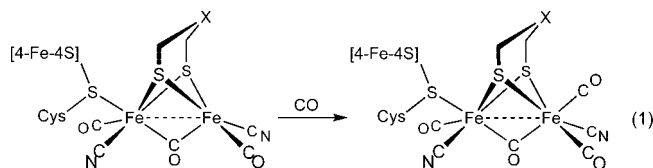
Although initial modeling efforts focused on the cyanide derivatives of $Fe_2(SR)_2(CO)_6$,[7] progress related to catalytic and structural aspects have mainly employed phosphine and carbene coligands.[8] The chief advantage of these abiological ligands derives from the adjustability of their steric and donor properties. Furthermore, the redox chemistry of the diiron dicyanides has proven difficult,[9] possibly due to the easy formation of μ-CN oligomers. Chemical oxidation of phosphine- and isocyanide-substituted Fe^IFe^I complexes affords diferrous derivatives containing μ-CO ligands.[9,10]

[†] University of Illinois at Urbana–Champaign.
[‡] University of Milano−Bicocca.

(1) De Lacey, A. L.; Fernández, V. M.; Rousset, M.; Cammack, R. *Chem. Rev.* **2007**, *107*, 4304–4330.

(2) Vignais, P. M.; Billoud, B. *Chem. Rev.* **2007**, *107*, 4206–4272.

(3) Justice, A. K.; Rauchfuss, T. B.; Wilson, S. R. *Angew. Chem., Int. Ed.* **2007**, *46*, 6152–6154.

(4) Liu, T.; Darensbourg, M. Y. *J. Am. Chem. Soc.* **2007**, *129*, 7008–7009.

(5) De Lacey, A. L.; Stadler, C.; Cavazza, C.; Hatchikian, E. C.; Fernandez, V. M. *J. Am. Chem. Soc.* **2000**, *122*, 11232–11233.

(6) Bennett, B.; Lemon, B. J.; Peters, J. W. *Biochemistry* **2000**, *39*, 7455–7460. Fontecilla-Camps, J. C.; Volbeda, A.; Cavazza, C.; Nicolet, Y. *Chem. Rev.* **2007**, *107*, 4273–4303.

(7) Schmidt, M.; Contakes, S. M.; Rauchfuss, T. B. *J. Am. Chem. Soc.* **1999**, *121*, 9736–9737. Le Cloirec, A.; Davies, S. C.; Evans, D. J.; Hughes, D. L.; Pickett, C. J.; Best, S. P.; Borg, S. *Chem. Commun.* **1999**, 2285–2286. Lyon, E. J.; Georgakaki, I. P.; Reibenspies, J. H.; Darensbourg, M. Y. *Angew. Chem., Int. Ed.* **1999**, *38*, 3178–3180.

(8) Kubas, G. J. *Chem. Rev.* **2007**, *107*, 4152–4205. Linck, R. C.; Rauchfuss, T. B. In *Bioorganometallics: Biomolecules, Labeling, Medicine*; Jaouen, G., Ed.; Wiley-VCH: Weinheim, 2005. Georgakaki, I. P.; Darensbourg, M. Y. *Comp. Coord. Chem. II* **2004**, *8*, 549–568.

(9) Boyke, C. A.; van der Vlugt, J. I.; Rauchfuss, T. B.; Wilson, S. R.; Zampella, G.; De Gioia, L. *J. Am. Chem. Soc.* **2005**, *127*, 11010–11018.

Models featuring the mixed-valence Fe^IFe^{II} oxidation state have been described, starting with the spectroscopic characterization of the type $[Fe_2(\mu\text{-}SR)_2(\mu\text{-}CO)(CO)_3(CN)_2(SR_2)]^-$.[11] This species replicates the entire first coordination sphere of the active site in the H_{ox}^{CO} state. Models for the H_{ox} state of the enzyme include $[Fe_2(S_2C_3H_6)(CO)_4(PMe_3)(Imes)]PF_6$[4] and $[Fe_2\text{-}(S_2C_2H_4)(CO)_3(PMe_3)(dppv)]BF_4$[3] (Imes = 1,3-bis(2,4,6-trimethylphenyl)imidazol-2-ylidene; dppv = *cis*-$Ph_2PCH=CHPPh_2$). The latter complex reversibly binds CO.[3] We were, however, unable to obtain single crystals of the CO adduct due to its lability. In contrast, H_{ox}^{CO} from *Desulfovibrio desulfuricans* is robust and loses the exogenous CO only upon photolysis.[12,13] The lability of $[Fe_2(S_2C_2H_4)(\mu\text{-}CO)(CO)_3(PMe_3)(dppv)]BF_4$ is attributable to the relatively low basicity of its donor ligand set, which features three phosphine ligands, whereas the diiron site in H_{ox}^{CO} is bound to two cyanide ligands and a [4Fe-4S] cluster (the coordination of the [4Fe-4S] cluster via a μ-thiolato ligand has been estimated to be slightly more basic than a dialkythioether in donor strength[14]).

In order to prepare more robust models for H_{ox}^{CO}, we turned to the *tetra*phosphine complex $Fe_2(S_2C_2H_4)(CO)_2(dppv)_2$ (**1**).[15] This dicarbonyl derivative is bulkier and more electron-rich (ν_{CO} = 1888, 1868 cm^{-1}) than the corresponding triphosphine $Fe_2(S_2C_2H_4)(CO)_3(PMe_3)(dppv)$ (ν_{CO} = 1957, 1902 cm^{-1}).[3] As we show below, this tetraphosphine complex is indeed readily oxidized to a state that allows one to structurally and spectroscopically characterize a model for H_{ox}^{CO}.

Results and Discussion

Oxidation of $Fe_2(S_2C_2H_4)(CO)_2(dppv)_2$. As previously observed for the related trisphosphine complex,[3] oxidation of MeCN solutions of tetraphosphine **1** with 2 equiv of $FcPF_6$ (Fc^+ = $Fe(C_5H_5)_2^+$) yielded the diferrous complex $[Fe_2(S_2C_2H_4)(\mu\text{-}CO)(CO)(dppv)_2(NCMe)](PF_6)_2$ (*unsym*-[**1**(NCMe)](PF$_6$)$_2$). The ^{31}P NMR spectrum of *unsym*-[**1**(NCMe)](PF$_6$)$_2$ indicated four nonequivalent phosphine ligands. We have described the crystallographic analysis of the closely related C_s-symmetric complex $[Fe_2(S_2C_2H_4)(\mu\text{-}CO)(CO)(PMe_3)_4(NCMe)]^{2+}$, which features a $Fe(NCMe)(PMe_3)_2$ center wherein the two phosphine ligands occupy the two basal sites with the NCMe ligand in an apical site.[16] A related geometry applies to *unsym*-[**1**(NCMe)]$^{2+}$: the diphosphine on the Fe(dppv)(CO) center is assumed to occupy the apical and one basal coordination site, as verified by subsequent reactions (see below).

The oxidation of **1** in MeCN solution afforded *unsym*-[**1**(NCMe)]$^{2+}$ regardless of the stoichiometry of the oxidant. For example, using only 1 equiv of $FcPF_6$, we observed the formation of a ~1:1 mixture of unreacted starting material and
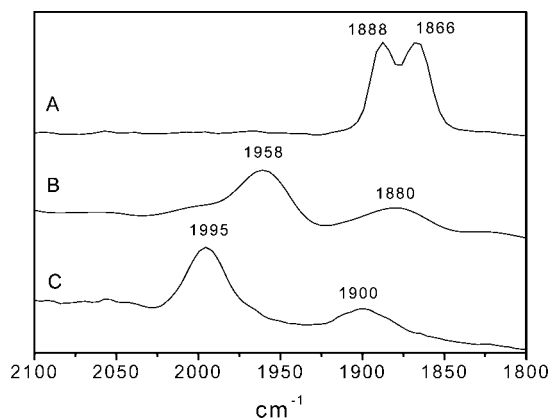

Figure 1. IR spectra of CH_2Cl_2 solutions (-45 °C) of $[Fe_2(S_2C_2H_4)\text{-}(CO)_2(dppv)_2]^z$ for $z = 0$ (A), $z = 1+$ (B), and $z = 2+$ (C), generated by addition of 1 equiv of $FcBF_4$ to **1** for $z = 1+$ and 2 equiv of $AcFcBF_4$ for $z = 2+$.

unsym-[**1**(NCMe)]$^{2+}$. Upon changing the solvent to CH_2Cl_2, the oxidation of **1** was, however, found to follow a different course, as only single-electron oxidations were observed. Indeed, electrochemical measurements on CH_2Cl_2 solutions of **1** showed a reversible oxidation at -175 mV (vs Ag/AgCl). When the electrochemical measurements were conducted under a CO atmosphere, two separate one-electron oxidation events were observed, at -195 and $+25$ mV, each of which is at least partially reversible.

Oxidation of **1** was conveniently effected using 1 equiv of $FcBF_4$ at -45 °C in CH_2Cl_2 solution. *In situ* IR measurements indicate that the oxidation product [**1**]$^+$ adopts a "rotated structure" characteristic of other H_{ox} models[3,4] (Figure 1). Specifically, this oxidation shifts the terminal ν_{CO} bands to higher energy by an average of 70 cm^{-1}; the band at 1880 cm^{-1} is assigned to a semibridging CO ligand. This *in situ* generated material was used in subsequent experiments. Because the product from one-electron oxidation has only limited stability, all synthetic operations were conducted near or below 0 °C.

Mixed-Valence CO Adducts, Models for H_{ox}^{CO}. Solutions of [**1**]$^+$ were found to rapidly absorb CO to give an adduct at -45 °C. The resulting IR spectrum featured ν_{CO} bands at 1970 and 1791 cm^{-1} (Figure 3). When this sample was allowed to warm to 0 °C, followed by cooling again to -45 °C, the terminal $\nu_{t\text{-}CO}$ band was shifted from 1970 to 1961 cm^{-1} (with a shoulder at ~1975 cm^{-1}), and the $\nu_{\mu\text{-}CO}$ band was shifted from 1791 to 1775 cm^{-1}. These results indicate isomerization of the cationic CO adduct.

Four diastereomers are possible for $[Fe_2(S_2C_2H_4)(\mu\text{-}X)\text{-}(CO)_2(dppv)_2]^+$ (Figure 2). The initial isomer is the unsymmetrical one, labeled *unsym*-[**1**(CO)]$^+$, wherein one dppv ligand spans apical/basal sites and the other dibasal sites. The structure is very similar to that assumed for [**1**]$^+$,[3] the immediate precursor to *unsym*-[**1**(CO)]$^+$. In the more stable isomer, *sym*-[**1**(CO)]$^+$, each dppv ligand chelates across apical/basal positions, as verified crystallographically (see below). The isomerization of *unsym*-[**1**(CO)]$^+$ to *sym*-[**1**(CO)]$^+$ at -30 °C in CH_2Cl_2 occurs efficiently, with no observable intermediates. When **1** was oxidized under CO at 0 °C, *sym*-[**1**(CO)]$^+$ formed exclusively. Samples of *sym*-[**1**(CO)] BF$_4$ were obtained in analytical purity.

The stability of the two isomers in solution is quite different. Upon removal of the CO atmosphere, *unsym*-[**1**(CO)]$^+$ quickly reverted to [**1**]$^+$ even at -45 °C. In contrast, solutions of *sym*-[**1**(CO)]$^+$ were stable even at room temperature for several

(10) Boyke, C. A.; Rauchfuss, T. B.; Wilson, S. R.; Rohmer, M.-M.; Bénard, M. *J. Am. Chem. Soc.* **2004**, *126*, 15151–15160.

(11) Razavet, M.; Borg, S. J.; George, S. J.; Best, S. P.; Fairhurst, S. A.; Pickett, C. J. *Chem. Commun.* **2002**, 700–701. Razavet, M.; Davies, S. C.; Hughes, D. L.; Barclay, J. E.; Evans, D. J.; Fairhurst, S. A.; Liu, X.; Pickett, C. J. *Dalton Trans.* **2003**, 586–595.

(12) Lemon, B. J.; Peters, J. W. *J. Am. Chem. Soc.* **2000**, *122*, 3793–3794. Chen, Z.; Lemon, B. J.; Huang, S.; Swartz, D. J.; Peters, J. W.; Bagley, K. A. *Biochemistry* **2002**, *41*, 2036–2043.

(13) Roseboom, W.; Lacey, A. L.; Fernandez, V. M.; Hatchikian, E. C.; Albracht, S. P. J. *J. Biol. Inorg. Chem.* **2006**, *11*, 102–118.

(14) Tard, C.; Liu, X.; Ibrahim, S. K.; Bruschi, M.; De Gioia, L.; Davies, S. C.; Yang, X.; Wang, L.-S.; Sawers, G.; Pickett, C. J. *Nature* **2005**, *433*, 610–614.

(15) Justice, A. K.; Zampella, G.; De Gioia, L.; Rauchfuss, T. B. *Chem. Commun.* **2007**, 2019–2021.

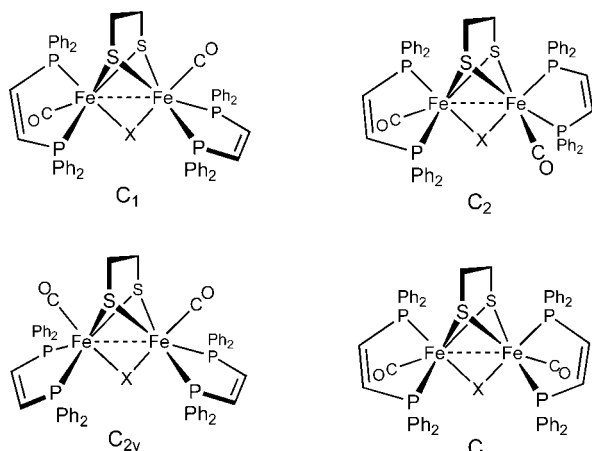(16) van der Vlugt, J. I.; Rauchfuss, T. B.; Wilson, S. R. *Chem. Eur. J.* **2005**, *12*, 90–98.

Figure 2. Isomers of [Fe₂(S₂C₂H₄)(μ-X)(CO)₂(dppv)₂].

Figure 4. Structure of the cation in *sym*-[Fe₂(S₂C₂H₄)(μ-CO)(CO)₂-(dppv)₂]BF₄, *sym*-[1(CO)]BF₄, with thermal ellipsoids set at the 35% probability level. Phenyl ellipsoids, phenyl hydrogen atoms, and the BF₄⁻ were omitted for clarity.

Figure 3. IR spectra of CH₂Cl₂ solutions at −45 °C of *unsym*-[Fe₂(S₂C₂H₄)-(μ-CO)(CO)₂(dppv)₂]⁺ (A) and *unsym*-[Fe₂(S₂C₂H₄)(μ-CO)(CO)(¹³CO)-(dppv)₂]⁺ (B). IR spectra of CH₂Cl₂ solutions at 0 °C of *sym*-[Fe₂(S₂C₂H₄)(μ-CO)(CO)₂(dppv)₂]⁺ (C) and *sym*-[Fe₂(S₂C₂H₄)(μ-CO)(CO)(¹³CO)(dppv)₂]⁺ (D).

minutes. The relative stability of solid samples of the two isomers matched the trend observed for solutions. Solid samples of *sym*-[1(CO)]BF₄ could be precipitated at 0 °C with hexanes. The purple powder exhibited an IR spectrum (solid KBr pellet) consistent with the solution data for *sym*-[1(CO)]BF₄. In contrast, precipitation of *unsym*-[1(CO)]BF₄ from CH₂Cl₂ solution gave a mixture, which based on IR analysis consisted of **1** and other species with ν_CO bands consistent with diferrous species. Dissolution of this precipitate in CH₂Cl₂ solution at −45 °C under an atmosphere of CO gave *unsym*-[1(CO)]BF₄, the result of an apparent comproportionation. The non-isolability of solid samples of *unsym*-[1(CO)]BF₄ and of [1]BF₄ reflects their very similar structures. The IR spectra (solid KBr pellets) of the solids precipitated from solutions of *unsym*-[1(CO)]BF₄ and [1]BF₄ are similar (see Supporting Information).

¹³CO Labeling Studies. The stereochemistry of the carbonylation was probed by conducting the aforementioned oxidation of **1** under an atmosphere of ¹³CO at −45 °C. This process afforded mainly a single isotopomer, *unsym*-[1(¹³CO)]⁺, as indicated by characteristic changes in the IR spectrum (Figure 3). Specifically, the single ν_CO band (1970 cm⁻¹) assigned to the pair of terminal CO ligands in *unsym*-[1(CO)]⁺ was split in *unsym*-[1(¹³CO)]⁺ to give absorptions at 1970 and 1933 cm⁻¹ (calculated: 1925 cm⁻¹). The band assigned to the bridging CO (1791 cm⁻¹) was unaffected by the isotopic labeling. When the
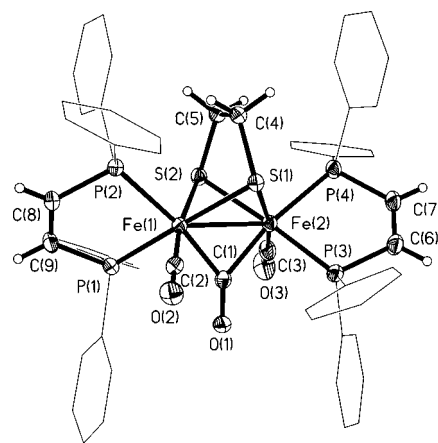
same oxidation of **1** under ¹³CO was conducted at 0 °C, we obtained *sym*-[1(¹³CO)]⁺. Once again, the terminal CO bands in *sym*-[1(CO)]⁺ are more split in the ¹³CO-labeled product (1972, 1926 cm⁻¹), and, again, the position of ν_{μ-CO} remained unaffected. Notice that ¹³CO does not affect the terminal Fe−¹²CO band (ν_{t-¹²CO}) for the *unsym* isomer: these terminal CO ligands reside on different metals and are mutually cisoid and thus weakly coupled. A similar lack of coupling is evident in the IR spectrum for the protein.[5] The ¹³CO-labeling results indicate that the *unsym*-to-*sym* rearrangement (eq 2) is stereospecific.

(2)
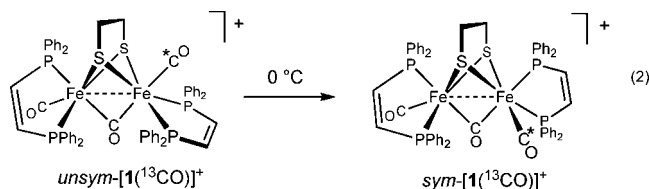
Crystallographic Characterization of *sym*-[1(CO)]X (X = BF₄, PF₆). Single crystals of *sym*-[1(CO)]BF₄ were obtained by slow diffusion of hexanes into a CO-saturated CH₂Cl₂ solution of the salt at −20 °C (Figure 4). The salt indeed corresponds to the anticipated stoichiometry with one BF₄⁻. The complex has crystallographically imposed C_2 symmetry: each dppv ligand is chelated to apical/basal sites on separate iron centers. The bridging CO is symmetrically positioned between the two Fe centers. In contrast, most complexes of the type [Feᴵᴵ₂(SR)₂L₆(μ-CO)] exhibit semibridging μ-CO ligands.[3,4,9,10,16,17] The most striking crystallographic result is the Fe−Fe distance, which is 2.7012(14) Å. The great majority of diiron dithiolato carbonyls, including many that are highly substituted, exhibit Fe−Fe distances in the range 2.53–2.60 Å. The previous record was 2.6006(7) Å for [Fe₂(S₂C₂H₄)(μ-CO)(CO)(PMe₃)₄(NCMe)]-(PF₆)₂.[16] The Fe−S bonds at 2.319 Å are also elongated relative to precedents where the Fe−S bond length are between 2.25 and 2.29 Å. The collective effect of the longer Fe−Fe and Fe−S bond lengths results in a more open Fe₂S₂ core. A table comparing bond distances and angles of *sym*-[1(CO)]⁺ with those of other Fe₂(SR)₂ complexes is given in the Supporting

(17) van der Vlugt, J. I.; Rauchfuss, T. B.; Whaley, C. M.; Wilson, S. R. *J. Am. Chem. Soc.* **2005**, *127*, 16012–16013.

Table 1. Selected Bond Distances (Å) and Angles (deg) for [**1**(CO)]BF$_4$ and [**1**(CO)]PF$_6$[a]

|	[**1**(CO)]BF$_4$	[**1**(CO)]PF$_6$
Fe−Fe	2.7012(14)	2.7065(13)
Fe−S (avg)	2.32	2.31
Fe−P^{apical} (avg)	2.34	2.35
Fe−P^{basal} (avg)	2.26	2.26
Fe−CO^{bridging} (avg)	1.97	1.98
Fe−CO^{terminal} (avg)	1.77	1.77
C−O^{bridging}	1.179(5)	1.179(8)
C−O^{terminal} (avg)	1.14	1.14
Fe−S−Fe (avg)	71.22	71.48
Fe−Fe−S (avg)	54.39	54.24
Fe−Fe−P^{apical} (avg)	141.27	141.91
Fe−Fe−P^{basal} (avg)	119.37	119.71
Fe−CO^{bridging}−Fe	86.16(18)	86.4(3)
Fe−Fe−CO^{basal} (avg)	117.00	116.45
Fe−C−O^{bridging}	136.95	136.80
Fe−C−O^{terminal}	178.35	177.25

[a] A more complete list of bond distance and angles is provided in the Supporting Information.
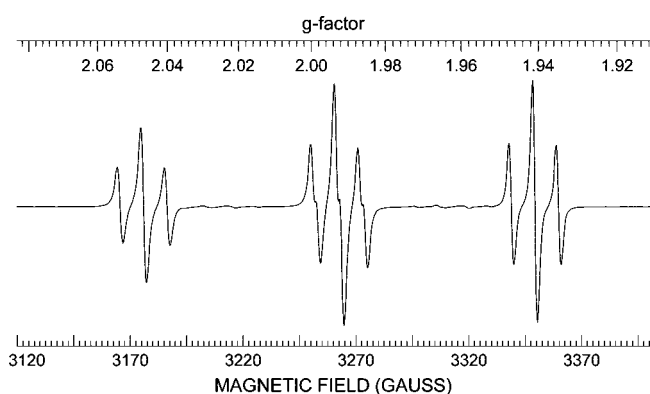
Figure 5. X-band EPR spectrum of *sym*-[**1**(CO)]$^+$ in 1:2 toluene:CH$_2$Cl$_2$ solution at 20 °C.

Information. The corresponding hexafluorophosphate salt *sym*-[**1**(CO)]PF$_6$ was also prepared and crystallographically characterized. The results for the two salts were almost identical (Table 1).

EPR Spectroscopy. The EPR spectrum of a solution of [**1**]$^+$ was broad, but those for *unsym*-[**1**(CO)]$^+$ and *sym*-[**1**(CO)]$^+$ were well resolved. These isotropic spectra all feature significant coupling to the phosphorus ligands. We supplemented these measurements with the EPR spectrum of [Fe$_2$(S$_2$C$_2$H$_4$)-(CO)$_3$(PMe$_3$)(dppv)]BF$_4$, which exhibits a similar triplet pattern consistent with its C_s-symmetry[18] and consistent with the localization of the spin on the rotated Fe^I(dppv) center. For the CO adducts, the splitting patterns correlate with the number of "apical" phosphine ligands, which are approximately trans to the Fe−Fe vector. The degree of delocalization is significant for these adducts, as indicated by the magnitude of the hyperfine coupling. Thus, the spectrum for *unsym*-[**1**(CO)]$^+$ consists of a doublet of quartets ($A(^{31}P)_{apical}$ = 287, $A(^{31}P)_{basal}$ ≈ 30 MHz), whereas the spectrum for *sym*-[**1**(CO)]$^+$ consists of a triplet of triplets ($A(^{31}P)_{apical}$ ≈ 240, $A(^{31}P)_{basal}$ ≈ 29 MHz) (Figures 5 and 6, Table 2). The significant difference in the *A* values for the apical vs basal phosphine ligands indicates that the SOMO in these complexes is aligned with the Fe−Fe vector, consistent

(18) Dehont, R.; Justice, A. K.; Münck, E.; Rauchfuss, T. B.,work in progress.
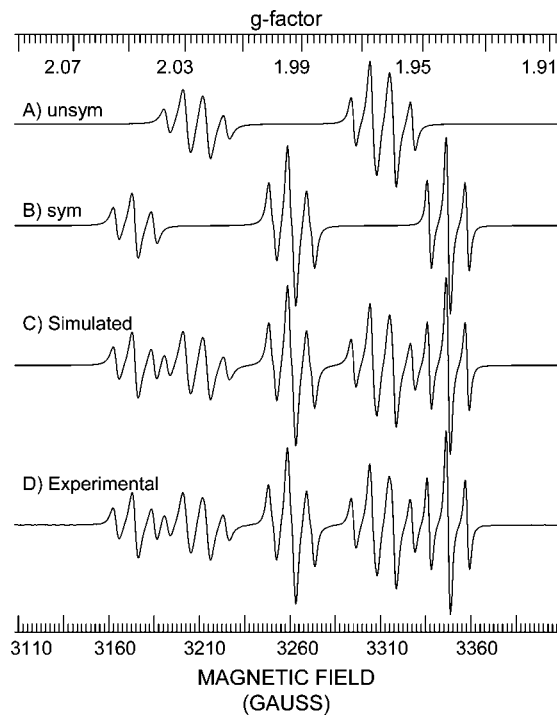
Figure 6. X-band EPR data and simulations for *unsym*-[**1**(CO)]$^+$ and *sym*-[**1**(CO)]$^+$ in a 1:2 toluene:CH$_2$Cl$_2$ solution at −30 °C: simulation of *unsym*-[**1**(CO)]$^+$ (A), simulation of *sym*-[**1**(CO)]$^+$ (B), simulation of a mixture of *unsym*- and *sym*-[**1**(CO)]$^+$ (C), and experimental spectrum of the mixture (D).

Table 2. EPR Parameters for *unsym*- and *sym*-[**1**(CO)]$^+$ Used in the Simulations

	sym-[Fe$_2$(S$_2$C$_2$H$_4$)-(μ-CO)(CO)$_2$(dppv)$_2$]$^+$	*unsym*-[Fe$_2$(S$_2$C$_2$H$_4$)-(μ-CO)(CO)$_2$(dppv)$_2$]$^{+b}$
g	1.9928	1.9935
$A(^{31}P)^a$	241, 241, 29, 29	287, 34, 28, 28

[a] Hyperfine matrix values in MHz; divide by 2.99 for cm^{-1}. [b] At −30 °C; unstable at higher temperatures.

with the results of the DFT calculations (see below). When a solution containing a mixture of *unsym*- and *sym*-[**1**(CO)]$^+$ was allowed to warm to 20 °C, the components assigned to *unsym*-[**1**(CO)]$^+$ vanished (see Supporting Information). For mononuclear Fe(I) phosphine complexes, e.g., *trans*-[Fe(CO)$_3$-(PPh$_3$)$_2$]$^+$, where the unpaired spin is localized in orbitals orthogonal to the P−Fe−P axis,[19] the hyperfine values are ca. 55 MHz, almost 2 times $A(^{31}P)_{basal}$ for diiron compounds.[20] Further analysis of the EPR spectra for frozen solutions is underway.[18]

Diferrous Derivatives. The oxidation of the mixed-valence derivatives provided information that supports the stereochemical assignments for the mixed-valence derivatives. Oxidation of a solution of *unsym*-[**1**(CO)]BF$_4$ with FcBF$_4$ at −45 °C gave *unsym*-[**1**(CO)]$^{2+}$. The solution IR spectrum of this *unsym*

(19) Therien, M. J.; Trogler, W. C. *J. Am. Chem. Soc.* **1986**, *108*, 3697–3702.

(20) Bagchizpr, R. N.; Bond, A. M.; Heggie, C. L.; Henderson, T. L.; Mocellin, E.; Seikel, R. A. *Inorg. Chem.* **1983**, *22*, 3007–3012. Blanch, S. W.; Bond, M. A.; Colton, R. *Inorg. Chem.* **1981**, *20*, 755. Baker, P. K.; Connelly, N. G.; Jones, B. M. R.; Maher, J. P.; Somers, K. R. *J. Chem. Soc., Dalton Trans.* **1980**, 579–585. MacNeil, J. H.; Chiverton, A. C.; Fortier, S.; Baird, M. C.; Hynes, R. C.; Williams, A. J.; Preston, K. F.; Ziegler, T. *J. Am. Chem. Soc.* **1991**, *113*, 9834–9842.

dication exhibits bands at 1896 (μ-CO), 2048, and 2024 cm^{-1}; these bands are shifted substantially to higher energy relative to those for the precursor. The ^{31}P NMR spectrum features four distinct peaks, confirming the unsymmetrical nature of this dication.

Oxidation of *sym*-[**1**(CO)]$^+$ gave *sym*-[**1**(CO)]$^{2+}$, which was also isolated as its BF$_4^-$ salt in analytical purity. The IR spectrum of *sym*-[**1**(CO)]$^{2+}$ features a $\nu_{\mu\text{-CO}}$ band at 1871 cm^{-1}, which is 25 cm^{-1} lower in energy than the *unsym* isomer, and a ν_{CO} band at 2015 cm^{-1} (see Supporting Information). The difference in the $\nu_{\mu\text{-CO}}$ is similar to the difference (16 cm^{-1}) for *sym*- vs *unsym*-[**1**(CO)]$^+$. For both Fe^I−Fe^{II} and Fe^{II}−Fe^{II} complexes, the bridging carbonyl frequency is highly dependent upon its trans ligands: the presence of a trans phosphine ligand lowers the energy of ν_{CO} by ca. 20 cm^{-1}. The two-line ^{31}P NMR spectrum for *sym*-[**1**(CO)]$^{2+}$ is consistent with C_2 symmetry. Both diferrous salts were obtained in analytical purity.

Solutions of *sym*-[**1**(CO)]$^{2+}$ in CD$_2$Cl$_2$ were observed to convert to *unsym*-[**1**(CO)]$^{2+}$ over the course of a few days. The isomerization of *sym*- to *unsym*-[**1**(CO)]$^{2+}$ proceeded only in the presence of light and was inhibited by an atmosphere of CO. Upon dissolution in MeCN, *unsym*-[**1**(CO)]$^{2+}$ converted rapidly into *unsym*-[**1**(NCMe)]$^{2+}$. Upon dissolving in MeCN, *sym*-[**1**(CO)]$^{2+}$ also converted into *unsym*-[**1**(NCMe)]$^{2+}$ but at a slower rate. The contrasting rates for interconversion of *sym* and *unsym* isomers reflect the increased kinetic inertness of the d^6,d^6 vs the d^6,d^7 derivatives. The exchange of a terminal CO ligand for MeCN shifts $\nu_{\mu\text{-CO}}$ to higher energy (*sym*, $\nu_{\mu\text{-CO}}$ = +39 cm^{-1}; *unsym*, $\nu_{\mu\text{-CO}}$ = +14 cm^{-1}). Ordinarily, substitution of the CO by MeCN shifts the remaining CO bands to lower energy. The sign of $\nu_{\mu\text{-CO}}$ is tentatively attributed to a change of the μ-CO ligand from a symmetrical to an unsymmetrical bridging mode.

The cyclic voltammogram of **1** showed two oxidations, one at potential less positive than the Fc$^{+/0}$ couple (−175 mV vs Ag/AgCl), and a second above the Fc$^{+/0}$ couple (+600 mV). Treatment of **1** with 2 equiv of [CpFe(C$_5$H$_4$Ac)]BF$_4$ (+270 mV vs Fc$^{+/0}$) resulted in complete consumption of the oxidant and the formation of a new species assigned as [**1**]$^{2+}$ (treatment of CH$_2$Cl$_2$ solutions of **1** with 2 equiv of FcBF$_4$ gave only [**1**]$^+$). The IR spectrum of the resulting solution resembled that for [**1**]$^+$, but the terminal and bridging CO bands were shifted to higher energy by 40 and 20 cm^{-1}, respectively (Figure 1). We suggest that this dication adopts a structure similar to that of [**1**]$^+$, wherein one Fe(dppv)(CO) site has rotated. The ^{31}P NMR spectrum confirms the low-symmetry structure: the pattern resembles that for *unsym*-[**1**(CO)]$^{2+}$. Treatment of this doubly oxidized species with CO gave *unsym*-[**1**(CO)]$^{2+}$ without the intermediacy of the *sym* isomer.

DFT Calculations. As a complement to the experimental results, simplified models of the isomers of [**1**(CO)]$^+$ and [**1**(CO)]$^{2+}$, in which pairs of PH$_3$ groups replaced each dppv ([**1**-PH$_3$(CO)]$^{n+}$), were evaluated by DFT calculations. Comparison of the structures of [**1**-PH$_3$(CO)]$^+$ and [**1**-PH$_3$(CO)]$^{2+}$ highlights two significant structural effects (Figure 7). First, a longer Fe−Fe distance is evident in monocationic species (2.666 Å for *sym*-[**1**-PH$_3$(CO)]$^+$ and 2.691 Å for *unsym*-[**1**-PH$_3$(CO)]$^+$ compared to 2.523 Å for *sym*-[**1**-PH$_3$(CO)]$^{2+}$ and 2.529 Å for *unsym*-[**1**-PH$_3$(CO)]$^{2+}$), indicating a weakened Fe−Fe bonding interaction, as expected also on the basis of the 18-electron rule. Second, the calculations revealed a stronger competition between the mutually trans μ-acceptor CO groups for the *unsym* isomer of the monocation in comparison to the dication. This unfavor-
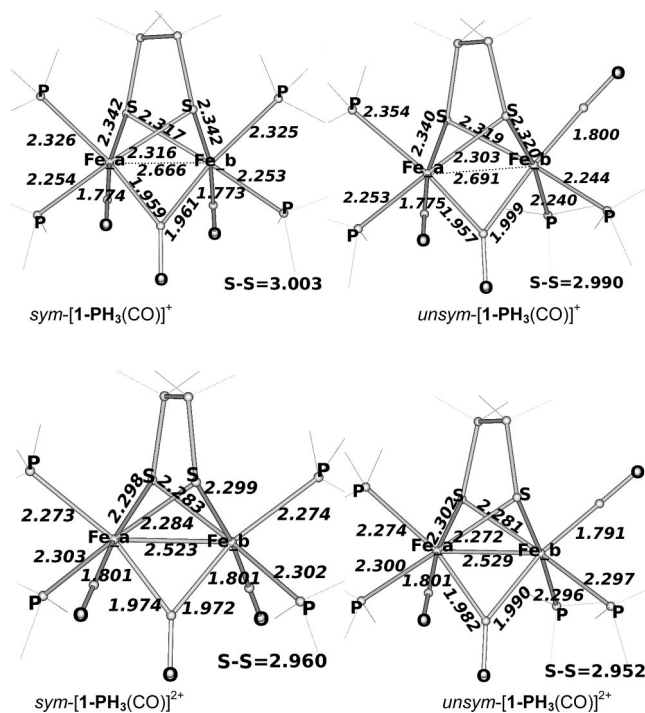
Figure 7. DFT structures of *sym*-[**1**-PH$_3$(CO)]$^+$, *unsym*-[**1**-PH$_3$(CO)]$^+$, *sym*-[**1**-PH$_3$(CO)]$^{2+}$, and *unsym*-[**1**-PH$_3$(CO)]$^{2+}$ (distances in Å).

Table 3. Computed Spin Densities for [**1**-PH$_3$(CO)]$^+$ Models

compound	Fe$_a$	Fe$_b$	P$_{basal}$	P$_{apical}$	S	CO
sym-[**1**-PH$_3$(CO)]$^+$	0.41	0.41	0.00	0.05	0.06	C: 0.01
					0.06	O: 0.04
unsym-[**1**-PH$_3$(CO)]$^+$	0.49	0.27	0.00	0.07	0.06	C: 0.04
					0.07	O: 0.06

able interaction in *unsym*-[**1**-PH$_3$(CO)]$^+$ is evident from Fe$_b$−C bond distances (Figure 7). In fact, due to this unfavorable interaction, *unsym*-[**1**-PH$_3$(CO)]$^+$ is computed to be slightly less stable than the corresponding *sym* isomer by 0.8 kcal/mol.

The analysis of the electronic structure of [**1**-PH$_3$(CO)]$^+$ reveals that the unpaired electron is more localized on Fe$_a$ (Table 3; see Figure 7 for Fe labeling) in the *unsym* isomer, whereas it is evenly distributed on both iron atoms in *sym*-[**1**-PH$_3$(CO)]$^+$. The SOMOs include contributions from Fe d$_{z^2}$ and π* μ-CO, as well as from atomic orbitals centered on S and apical P atoms (Figure 8).

The DFT study shows that the Fe−Fe bond is strengthened in the [**1**-PH$_3$(CO)]$^{2+}$ isomers, as indicated by the contraction calculated for the Fe−Fe distances (Figure 7). In contrast to the case for the monocation, the *unsym* isomer of the dication is the more stable of the two, although by only 0.6 kcal/mol, in agreement with experimental findings. The enhanced stability of the *unsym* isomer in the dicationic species stems from the diminished significance of the unfavorable competition between the mutually trans CO groups in the dication vs the monocation. In fact, competition between the two CO groups bound to Fe$_b$ elongates the Fe$_b$−C bond distances by 0.064 Å moving from *sym*- to *unsym*-[**1**-PH$_3$(CO)]$^+$ isomers, in which the Fe valence electrons are not involved in a Fe−Fe bond. Due to the presence of the Fe−Fe bond in [**1**-PH$_3$(CO)]$^{2+}$ (which can be viewed as a seventh ligand in the Fe coordination spheres), the elongation of Fe$_b$−C bond distances upon moving from *sym* to *unsym* is

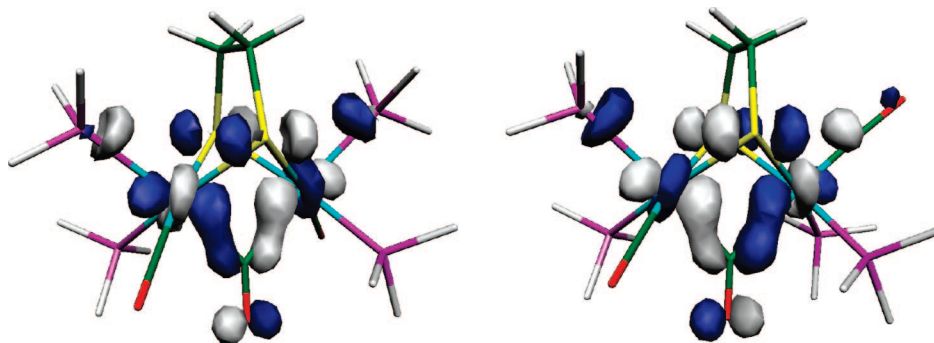**Figure 8.** SOMO of *sym*-[**1-PH₃**(CO)]⁺ (left) and *unsym*-[**1-PH₃**(CO)]⁺ (right). Cutoff value = 0.03.

only 0.008 Å, indicating that back-donation from Fe$_b$ to CO occurs irrespective of the trans CO ligands. It should also be noted that in *unsym* isomers the unfavorable steric interactions between the PH₃ groups and dithiolate are relieved.

Discussion

The complex Fe₂(S₂C₂H₄)(CO)₂(dppv)₂ can be oxidized to yield spectroscopic and structural models relevant to the active site of the H$_{ox}$ and H$_{ox}^{CO}$ states of the [FeFe]-hydrogenases. One equivalent of oxidant in a noncoordinating solvent generates an unstable 33e⁻ [Fe₂(SR)₂(CO)₂(dppv)₂]⁺ species that binds CO reversibly to give a 35e⁻ adduct electronically related to H$_{ox}^{CO}$.[1] This species isomerizes to give a thermally robust symmetrical derivative, the *sym* isomer, that is valence-delocalized. Using ¹³CO, we verified that the exogenous CO binds to the apical site and that the isomerization is intramolecular. *In situ* IR spectroscopy showed that [Fe₂(S₂C₂H₄)-(CO)₂(dppv)₂]⁺ does not bind H₂, which is not surprising since the kinetic (*unsym*) isomer of [Fe₂(S₂C₂H₄)(μ-CO)(CO)₂-(dppv)₂]⁺ is thermally fragile. Carbon monoxide invariably binds strongly to metal centers that form dihydrogen adducts; thus, the tendency of a complex to form a robust CO adduct is a prerequisite for the binding/activation of H₂.[21]

The isomeric 35e⁻ derivatives [Fe₂(S₂C₂H₄)(μ-CO)(CO)₂-(dppv)₂]⁺ both undergo further one-electron oxidation to afford diamagnetic 34e⁻ dications. Although the third CO shifts the redox potential of the diiron unit substantially (~700 mV), the shift is insufficient to induce disproportionation to diferrous and (Fe^I)₂ products. With better donors such as MeCN, these 35e⁻ adducts are a stronger reductant than the parent 34e⁻ species, and disproportionation ensues, inhibiting the isolation of mixed-valence derivatives. The conversion of the 35e⁻ H$_{ox}^{CO}$ models to diamagnetic diferrous species has allowed the stereochemistry to be further corroborated by ³¹P NMR spectroscopy. We verified that the oxidations proceed with stereochemical retention since we obtained both the thermodynamic and kinetic isomers (Scheme 1).

The availability of two isomers of the CO adducts provides insights into the factors that influence the lability of the exogenous CO. In the kinetic *unsym* isomer, which is more similar to the H$_{ox}^{CO}$, the exogenous CO is trans to μ-CO and is labile even at low temperatures, whereas the thermodynamic isomer is more thermally robust because the μ-CO is trans to phosphine ligands. Treating the enzyme obtained from *D. desulfuricans (Dd)* with ¹³CO, De Lacey et al. had shown that the exogenous CO is not vibrationally coupled to the CO on

Scheme 1. Compounds Examined in This Work, with Selected IR Data
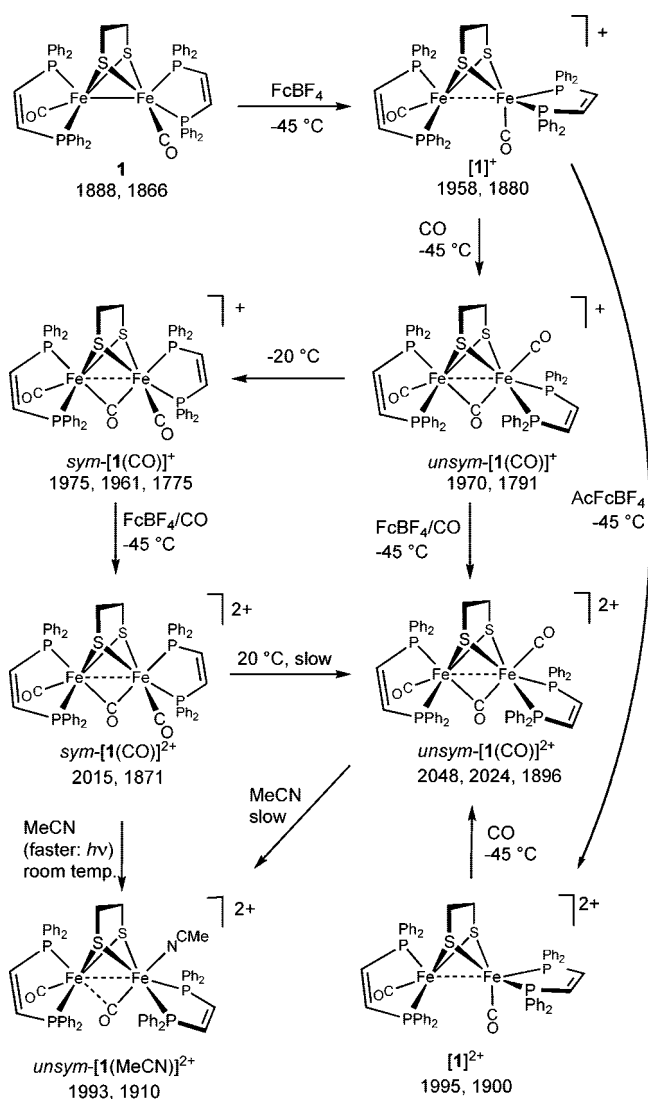
the second Fe center.[5] Indeed isotopic labeling indicates no coupling between the terminal CO ligands in *unsym*-[**1**(CO)]⁺.

The most striking crystallographic result is the elongated Fe–Fe distance of 2.70 Å for a mixed-valence 35e⁻ diiron complex. Diiron(I) dithiolato carbonyls display a narrow range of Fe–Fe distances near 2.55 Å.[22] The distances elongate for

(21) Kubas, G. J. *Metal Dihydrogen and μ-Bond Complexes*; Kluwer Academic/Plenum: New York, 2001.

(22) Evans, D. J.; Pickett, C. J. *Chem. Soc. Rev.* **2003**, *32*, 268–275.

complexes with bridging or semibridging CO ligands, where the Fe−Fe distances are 2.5–2.65 Å.[4,9,10,23] In their crystallographic characterization of the CO-inhibited form of hydrogenase I from *Clostridium pasteurianum*, Lemon et al. confirmed the presence of a CO ligand at the apical site of the distal Fe. No change was observed in Fe−Fe distance for reasons that might be attributable to limited resolution of the data.[24,25] Theory predicts modest changes in the Fe_2S_2 tetrahedrane for the H_{ox} and H_{red} states,[25] yet it is the Fe−S and Fe−Fe distances that are most reliably obtained from the structural biology. The one state for which this core is predicted to change significantly is H_{ox}^{CO}. On the basis of DFT calculations, Liu and Hu predicted a Fe−Fe distance of 2.633 Å for H_{ox}^{CO}.[26]

With models converging on the description of H_{ox} and H_{ox}^{CO} as $Fe^I Fe^{II}$ species,[3,4] the assignment of the Fe^{II} and Fe^I sites has become topical.[25,27,28] Noteworthy is the unchanging energy for the ν_{CO} band for proximal FeCO (1965 cm^{-1}, enzymes isolated from *Desulfovibrio vulgaris* and *Dd*[1,13]) in both the H_{red} and H_{ox} states.[29] This result would be consistent with the proximal iron center being redox-invariant.[27] *All* CO bands in our and related complexes shift upon oxidation, so no model simulates this biophysical result. IR data for the *Dd* enzyme[5] support a 1+ oxidation state for the distal Fe in H_{ox} since ν_{CO} for this iron (1940 cm^{-1}) is lower in energy than ν_{CO} for the proximal FeCO (1965 cm^{-1}).[22] On the basis of their spectroscopic analysis of the hydrogenase from *Dd*, Lubitz and co-workers found that, for both the H_{ox} and H_{ox}^{CO} states, the unpaired spin is distributed over the two iron centers in addition to the [4Fe-4S] cluster. They assign the proximal iron as Fe^I in the H_{ox}, H_{red}, and H_{ox}^{CO} states.[27,29] Our and Darensbourg's models for H_{ox} are more consistent with the proximal iron being Fe^{II}.[30] Consistent with Lubitz's analysis, our EPR results indicate that our models for the H_{ox}^{CO} state are more delocalized, with $(Fe^{1.5+})_2$ character, as indicated by the values of $A(^{31}P)$ for both the *sym* and *unsym* isomers. The differences between the model systems and the interpretation of the biophysical data may reflect deficiencies in the models, which lack biological ligands and clearly lack many of the second coordination sphere effects that may be energetically significant.[31] Certain mechanistic advantages would, however, result from our model: the diiron subunit in H_{ox} "sequesters" the Lewis acidic Fe^{II} center at the coordinatively saturated proximal site until substrate binding, whereupon intramolecular electron transfer relocates some Fe^{II} character to the distal site, which binds and acidifies H_2, leading to heterolytic activation (eq 3).

$$(3)$$
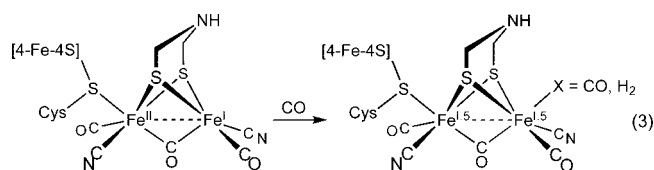
Although further work is indicated, it is clear from this and related studies[3,4,32] that, using appropriate ligand sets, the

chemistry of mixed-valence diiron dithiolates can be rich and relatively controllable. The properties of these bimetallic systems will be further discussed in the future.

Experimental Section

Unless otherwise indicated, reactions were conducted using Schlenk techniques at reduced temperatures, and reagents were purchased from Aldrich. Solvents were either HPLC-grade and purified using an alumina filtration system (Glasscontour Co., Irvine, CA) or distilled under nitrogen over CaH_2. Commercial $FcBF_4$ (Aldrich) was recrystallized before use. $[CpFe(C_5H_4Ac)]BF_4$ was prepared by literature methods.[33] The diiron complex Fe_2-$(S_2C_2H_4)(CO)_2(dppv)_2$ has been described.[15] ^{13}CO was obtained from Aldrich (99 atom% ^{13}CO; <5 atom % ^{18}O). NBu_4PF_6 (Aldrich) was recrystallized from methylene chloride and hexane. NMR spectra were recorded at room temperature on a Varian Mercury 500 MHz spectrometer (202 MHz for ^{31}P). NMR chemical shifts are quoted in ppm; spectra are referenced to TMS for ^1H and 85% H_3PO_4 for $^{31}P\{^1H\}$ spectra.

IR Spectroscopy. FT-IR spectra were recorded on a Mattson Infinity Gold FTIR spectrometer. *In situ* IR data were collected on a ReactIR 4000 (Mettler Toledo) with a silicon *in situ* probe (SiComp) and a four-bend arm. The reactor consisted of a specially modified pear-shaped 50-mL Schlenk flask. One sidearm was fitted to a source of N_2, the IR probe was inserted with a Teflon adaptor through the center 24/29 neck, and a second sidearm was fitted with a septum for injection of reagents. ReactIR 4000 experiments were performed in a similar manner as follows: In an inert atmosphere glovebox, the flask was charged with a precisely weighed sample of solid $Fe^I_2(S_2C_2H_4)(CO)_{6-x}(PR_3)_x$ (ca. 50 mg) and a Teflon-coated magnetic stir bar. After the flask was fitted with septa and removed from the box, 5.0 mL of CH_2Cl_2 was added through the middle septum, with care to rinse the sample into the bottom of the flask. The ReactIR probe was then inserted under a purge of N_2 gas. An initial IR spectrum was recorded over the range 4400–650 cm^{-1}. The flask was immersed in a slush of MeCN (mp −45 °C) or an ice bath (0 °C) on a magnetic stir plate. After the reactor was allowed to thermally equilibrate for several minutes, the IR spectrum was rerecorded. The remainder of the experiment varied as described below or in the figure captions.

Electrochemistry. Cyclic voltammetry was performed on a BAS CV-50W voltammetric analyzer. The following conditions were used: 0.1 M NBu_4PF_6 as the supporting electrolyte, glassy carbon as working electrode, Ag/AgCl in saturated KCl as reference electrode, Pt wire as counter electrode, analyte concentration 10^{-3} M.

DFT Calculations. DFT calculations were carried out using the BP86 functional[34] and a valence triple-ζ basis set with polarization on all atoms (TZVP).[35]

X-ray Crystallography. Crystals were mounted to a thin glass fiber using Paratone-N oil (Exxon). Data, collected at 198 K on a Siemens CCD diffractometer, were filtered to remove statistical outliers. The integration software (SAINT) was used to test for crystal decay as a bilinear function of X-ray exposure time and sin(θ). The data were solved using SHELXTL by direct methods; atomic positions were deduced from an E map or by an unweighted

(23) Tard, C.; Liu, X.; Hughes, D. L.; Pickett, C. J. *Chem. Commun.* **2005**, 133–135.

(24) Lemon, B. J.; Peters, J. W. *Biochemistry* **1999**, *38*, 12969–12973.

(25) Siegbahn, P. E. M.; Tye, J. W.; Hall, M. B. *Chem. Rev.* **2007**, *107*, 4414–4435.

(26) Liu, Z.-P.; Hu, P. *J. Am. Chem. Soc.* **2002**, *124*, 5175–5182.

(27) Lubitz, W.; Reijerse, E.; van Gastel, M. *Chem. Rev.* **2007**, *107*, 4331–4365.

(28) Fiedler, A. T.; Brunold, T. C. *Inorg. Chem.* **2005**, *44*, 9322–9334.

(29) Silakov, A.; Reijerse, E. J.; Albracht, S. P. J.; Hatchikian, E. C.; Lubitz, W. *J. Am. Chem. Soc.* **2007**, *129*, 11447–11458.

(30) Thomas, C. M.; Darensbourg, M. Y.; Hall, M. B. *J. Inorg. Biochem.* **2007**, *101*, 1752–1757.

(31) Greco, C.; Bruschi, M.; Heimdal, J.; Fantucci, P.; De Gioia, L.; Ryde, U. *Inorg. Chem.* **2007**, *46*, 7256–7258.

(32) Cheah, M. H.; Tard, C.; Borg, S. J.; Liu, X.; Ibrahim, S. K.; Pickett, C. J.; Best, S. P. *J. Am. Chem. Soc.* **2007**, *129*, 11085–11092. Best, S. A.; Borg, S. J.; White, J. M.; Razavet, M.; Pickett, C. J. *Chem. Commun.* **2007**, 4348–4350.

(33) Connelly, N. G.; Geiger, W. E. *Chem. Rev.* **1996**, *96*, 877–922.

(34) Becke, A. D. *J. Chem. Phys.* **1986**, *84*, 4524–4529. Perdew, J. P. *Phys. Rev.* **1986**, *B33*, 8882.

(35) Schaefer, A.; Huber, C.; Ahlrichs, R. *J. Chem. Phys.* **1994**, *100*, 5829–5835.

Table 4. Details of Crystallographic Data Collection and Structure Refinement for *sym*-[**1**(CO)]BF$_4$ and *sym*-[**1**(CO)]PF$_6$

	sym-[**1**(CO)]BF$_4$	*sym*-[**1**(CO)]PF$_6$
chemical formula	C$_{57}$H$_{48}$BO$_3$F$_4$P$_4$S$_2$Fe$_2$	C$_{57}$H$_{48}$O$_3$F$_6$P$_5$S$_2$Fe$_2$
temperature (K)	193 (2)	193 (2)
crystal size (mm^3)	0.70 × 0.52 × 0.20	0.27 × 015 × 0.14
crystal system	triclinic	triclinic
space group	$P\bar{1}$	$P\bar{1}$
a (Å)	10.614(6)	10.5296(9)
b (Å)	15.276(9)	16.4228(14)
c (Å)	22.765(13)	19.2603(16)
α (°)	97.618(9)	88.476(6)
β (°)	94.054(9)	74.783(5)
γ (°)	100.371(9)	86.220(5)
V (Å^3)	3582(4)	3206.7(5)
Z	1	2
density calcd (Mg·m^{-3})	1.437	1.533
μ (Mo Kα, mm^{-1})	0.71073	0.71073
max/min transitions	0.8401/0.5361	0.9271/0.8499
reflxs measd/indep	36978/13040	38551/12128
data/restraints/params	13040/336/895	12128/562/789
GOF on F^2	1.038	1.041
R_{int}	0.0340	0.1068
R1 [$I > 2\sigma$] (all data)^a	0.0594 (0.0836)	0.0829 (0.1456)
wR2 [$I > 2\sigma$] (all data)^b	0.1778 (0.1936)	0.2139 (002573)
max peak/hole (e$^-$/Å^3)	1.329/−1.115	1.119/−1.316

^{a} R1 = $\sum F_o - F_c/\sum F_o$. ^{b} wR2 = $\{[w(F_o - F_c)^2]/\sum[wF_o^2]\}^{1/2}$, where $w = 1/\sigma^2(F_o)$.

difference Fourier synthesis. H atom U values were assigned as 1.2U_{eq} for adjacent C atoms. Non-H atoms were refined anisotropically. Successful convergence of the full-matrix least-squares refinement of F^2 was indicated by the maximum shift/error for the final cycle (Table 4).

EPR Spectroscopy. X-band EPR spectra were collected on a Varian E-122 spectrometer. Variable-temperature spectra were recorded using an E-257 variable-temperature accessory using liquid nitrogen as a coolant. The magnetic fields were calibrated with a Varian NMR Gauss meter, and the microwave frequency was measured with a EIP frequency meter. EPR spectra were simulated with the program SIMPOW6.[36] The sample was flame-sealed under vacuum in a 3 × 4 mm quartz tube at liquid nitrogen temperatures. EPR samples were generated *in situ*, the following procedure being illustrative: a solution of 0.015 g (0.0142 mmol) of Fe$_2$(S$_2$-C$_2$H$_4$)(CO)$_2$(dppv)$_2$ in a mixture of 5 mL of CH$_2$Cl$_2$ and 5 mL of toluene at a low temperature (0 or −78 °C) was treated with a solution of 0.004 g (0.0142 mmol) of FcBF$_4$ in 5 mL of CH$_2$Cl$_2$. The resulting solution (1 mM) was transferred via cannula to a chilled (−78 °C) EPR tube that had been purged with N$_2$. The EPR tube was frozen in liquid nitrogen and flame-sealed under vacuum. For CO adducts, the Fe$_2$(S$_2$C$_2$H$_4$)(CO)$_2$(dppv)$_2$ solutions and EPR tubes were purged with CO for 15 min before addition of solution and for 2 min after solution was added.

[Fe$_2$(S$_2$C$_2$H$_4$)(μ-CO)(CO)(dppv)$_2$(NCMe)](PF$_6$)$_2$, *unsym*-[1**(NC-Me)](PF$_6$)$_2$.** A slurry of 0.100 g (0.0950 mmol) of **1** in 15 mL of MeCN at −30 °C was treated with a solution of 0.062 g (0.190 mmol) of FcPF$_6$ in 5 mL of MeCN. The reaction mixture was allowed to warm to room temperature, and solvent was removed in vacuum. The red-brown solid was redissolved in 10 mL of CH$_2$Cl$_2$, and the product precipitated out upon addition of 60 mL of hexanes. Yield: 0.096 g (73%). IR (MeCN): ν_{CO} = 1993, 1910 cm^{-1}. ^{1}H NMR (500 MHz, MeCN-d_3): δ 8.7–7.1 (m, 40H, C$_6$H$_5$), 6.4 (m, 4H, PCH), 2.7 (bs, 1H, SCH_2), 2.3 (bs, 1H, SCH_2), 2.1 (bs, 2H, SCH_2). ^{31}P NMR (MeCN-d_3): δ 95.7 (s), 73.6 (t, J_{P-P} = 5 Hz), 70.9 (d, J_{P-P} = 5 Hz), 69.0 (s), −143.8 (septet, PF$_6^-$). ESI-MS: *m/z* 1238.5 ([Fe$_2$(S$_2$C$_2$H$_4$)(CO)$_2$(dppv)$_2$(NCMe)]PF$_6^+$), 546.9

(36) Nilges, M. J.; Matteson, K.; L., B. R. *SIMPOW6*: A software package for the simulations of ESR powder-type spectra in ESR Spectroscopy in Membrane Biophysis.

([Fe$_2$(S$_2$C$_2$H$_4$)(CO)$_2$(dppv)$_2$(NCMe)]$^{2+}$). Anal. Calcd for C$_{58}$H$_{51}$-F$_{12}$Fe$_2$NO$_2$P$_6$S$_2$ (found): C, 50.35 (50.53); H, 3.72 (3.78); N, 1.01 (1.12).

[Fe$_2$(S$_2$C$_2$H$_4$)(CO)$_2$(dppv)$_2$]BF$_4$, [1**]BF$_4$.** A solution of 0.050 g (0.0475 mmol) of **1** in 7 mL of CH$_2$Cl$_2$ at −45 °C was treated with a solution of 0.013 g (0.0475 mmol) of FcBF$_4$ in 2 mL of CH$_2$Cl$_2$. Due to the instability of [**1**]BF$_4$, all data were collected *in situ*. IR (CH$_2$Cl$_2$): ν_{CO} = 1958, 1880 cm^{-1}.

***unsym*- and *sym*-[Fe$_2$(S$_2$C$_2$H$_4$)(μ-CO)(CO)$_2$(dppv)$_2$]BF$_4$, [**1**-(CO)]BF$_4$.** A solution of 0.100 g (0.095 mmol) of **1** in 20 mL of CH$_2$Cl$_2$ at −45 °C was treated with a solution of 0.026 g (0.095 mmol) of FcBF$_4$ in 10 mL of CH$_2$Cl$_2$ under an atmosphere of CO (ν_{CO} = 1970, 1791 cm^{-1}). The resulting purple solution was transferred into 300 mL of hexanes cooled to −78 °C, to precipitate the red-green-colored product. The solid featured bands for both **1** (ν_{CO} = 1889, 1870 cm^{-1}) and other species (ν_{CO} = 2020, 1947 cm; see Supporting Information). Dissolution of the precipitate in precooled (−45 °C) CH$_2$Cl$_2$ under an atmosphere of CO gave *unsym*-[**1**(CO)]BF$_4$ which, when redissolved in precooled (−45 °C) CH$_2$Cl$_2$ without CO, gave [**1**]BF$_4$ as the exclusive product.

When a CH$_2$Cl$_2$ solution of *unsym*-[**1**(CO)]BF$_4$ was layered with hexane and stored at −20 °C for several days, we obtained crystals of *sym*-[**1**(CO)]BF$_4$. Crystals were isolated by filtration. The solid was dried in a vacuum, and a solid IR sample (KBr) was prepared in a N$_2$ glovebox. IR revealed the presence of both *sym*-[**1**(CO)]BF$_4$ and *unsym*-[**1**(CO)]BF$_4$ isomers (ν_{CO} = 1973, 1961, 1798, 1773 cm^{-1}; see Supporting Information). The *sym* isomer was obtained in analytical purity (see below).

^{13}CO-Labeling of *unsym*-[1**(CO)]BF$_4$.** A solution of 0.050 g (0.0475 mmol) of **1** in 7 mL of CH$_2$Cl$_2$ at −45 °C was treated with a solution of 0.013 g (0.0475 mmol) of FcBF$_4$ in 2 mL of CH$_2$Cl$_2$under an atmosphere of ^{13}CO. IR (CH$_2$Cl$_2$): ν_{CO} = 1970, 1933 (^{13}CO), 1791 cm^{-1} (see Figure 2).

sym-[Fe$_2$(S$_2$C$_2$H$_4$)(μ-CO)(CO)$_2$(dppv)$_2$]BF$_4$, *sym*-[1**(CO)]BF$_4$.** A solution of 0.100 g (0.095 mmol) of **1** in 20 mL of CH$_2$Cl$_2$ at 0 °C was treated with a solution of 0.026 g (0.095 mmol) of FcBF$_4$ in 10 mL of CH$_2$Cl$_2$ under an atmosphere of CO. IR: ν_{CO} = 1975 (sh), 1961, 1775 cm^{-1} (see Figure 2). The resulting purple solution was transferred into 300 mL of hexanes precooled to −78 °C to precipitate the purple-colored product. Yield: 0.069 g (63%). IR (KBr): ν_{CO} = 1952, 1766 cm^{-1}. Anal. Calcd for C$_{57}$H$_{48}$-BF$_4$Fe$_2$O$_3$P$_4$S$_2$·CH$_2$Cl$_2$ (found): C, 55.62 (55.85); H, 4.02 (4.26). As tested by EPR and IR spectroscopy, solutions of this compound remain unchanged at room temperature for several minutes.

^{13}CO-Labeling of *sym*-[1**(CO)]BF$_4$.** A solution of 0.500 g (0.0475 mmol) of **1** in 7 mL of CH$_2$Cl$_2$ at 0 °C was treated with a solution of 0.013 g (0.0475 mmol) of FcBF$_4$ in 2 mL of CH$_2$Cl$_2$ under an atmosphere of ^{13}CO. IR (CH$_2$Cl$_2$): ν_{CO} = 1972, 1926 (^{13}CO), 1775 cm^{-1}.

sym-[Fe$_2$(S$_2$C$_2$H$_4$)(μ-CO)(CO)$_2$(dppv)$_2$]PF$_6$, *sym*-[1**(CO)]PF$_6$.** This preparation was modeled after the procedure for the BF$_4$ salt, using FcPF$_6$. Crystals were grown by slow diffusion of hexanes into a CO-saturated CH$_2$Cl$_2$ chloride solution at −20 °C.

Conversion of *unsym*-[1**(CO)]BF$_4$ to *sym*-[**1**(CO)]BF$_4$.** A solution of 0.050 g (0.0475 mmol) of **1** in 7 mL of CH$_2$Cl$_2$ at −30 °C was treated with a solution of 0.013 g (0.0475 mmol) of FcBF$_4$ in 2 mL of CH$_2$Cl$_2$ under an atmosphere of CO. The reaction was monitored *in situ*. The initial peaks were assigned to *unsym*-[**1**(CO)]BF$_4$ (1970, 1791 cm^{-1}). Over the course of 2 min, the *in situ* IR spectrum showed the disappearance of *unsym*-[**1**(CO)]BF$_4$ and the appearance of new peaks for *sym*-[**1**(CO)]BF$_4$ (1961, 1775 cm^{-1}).

***unsym*-[Fe$_2$(S$_2$C$_2$H$_4$)(μ-CO)(CO)$_2$(dppv)$_2$](BF$_4$)$_2$, *unsym*-[**1**-(CO)](BF$_4$)$_2$.** A solution of 0.100 g (0.095 mmol) of **1** in 10 mL of CH$_2$Cl$_2$ at −45 °C was treated with a solution of 0.052 g (0.190 mmol) of FcBF$_4$ in 10 mL of CH$_2$Cl$_2$ under a CO atmosphere. The solution was warmed to room temperature, and the red-brown product precipitated upon addition of 50 mL of CO-purged hexanes. Yield: 0.90 mg (76%). IR (CH$_2$Cl$_2$): ν_{CO} = 2048, 2024, 1896 cm^{-1}. ^{1}H NMR (500 MHz, CD$_2$Cl$_2$): δ 8.7–7.1 (m, 40H, C$_6$H$_5$), 6.4 (m,

4H, PC*H*), 3.4 (bs, 1H, SC*H$_2$*), 3.1 (bs, 1H, SC*H$_2$*), 2.4 (bs, 1H, SC*H$_2$*), 1.7 (bs, 1H, SC*H$_2$*). ^{31}P NMR (CD$_2$Cl$_2$): δ 91.4 (s), 72.8 (s), 69.9 (s), 67.6 (s). Anal. Calcd for C$_{57}$H$_{48}$B$_2$F$_8$Fe$_2$O$_3$P$_4$S$_2$ (found): C, 54.58 (54.19); H, 3.86 (3.86).

sym-[Fe$_2$(S$_2$C$_2$H$_4$)(μ-CO)(CO)$_2$(dppv)$_2$](BF$_4$)$_2$, sym-[1(CO)]-(BF$_4$)$_2$. A solution of 0.100 g (0.095 mmol) of **1** in 10 mL of CH$_2$Cl$_2$ at 0 °C was treated with a solution of 0.026 g (0.095 mmol) of FcBF$_4$ in 5 mL of CH$_2$Cl$_2$ under a CO atmosphere. After 10 min the reaction mixture was treated with 0.026 g (0.095 mmol) of FcBF$_4$ in 5 mL of CH$_2$Cl$_2$, maintaining the temperature at 0 °C and the CO atmosphere. The red-brown-colored solution was allowed to warm to room temperature, and the red-brown product precipitated upon addition of 60 mL of hexanes. Yield: 0.092 g (77%). IR (CH$_2$Cl$_2$): $ν_{CO}$ = 2015, 1871 cm^{-1}. ^{1}H NMR (500 MHz, CD$_2$Cl$_2$): δ 8.3–7.4 (m, 40H, C$_6$H$_5$), 7.0 (m, 4H, PC*H*), 1.7 (bs, 2H, SC*H$_2$*), 1.6 (bs, 2H, SC*H$_2$*). ^{31}P NMR (CD$_2$Cl$_2$): δ 86.2 (s), 81.8 (s). Anal. Calcd for C$_{57}$H$_{48}$B$_2$F$_8$Fe$_2$O$_3$P$_4$S$_2$ (found): C, 54.58 (54.77); H, 3.86 (3.90).

Isomerization of sym-[1(CO)](BF$_4$)$_2$ to unsym-[1(CO)](BF$_4$)$_2$. A J-Young NMR tube was charged with 0.005 g (0.004 mmol) of *unsym*-[**1**(CO)](BF$_4$)$_2$, 1 mL of CD$_2$Cl$_2$ was distilled into the J-Young tube at 78 K, and then the contents were allowed to warm to room temperature. Under ambient fluorescent lighting, the solution was observed to isomerize to the *unsym* isomer, as monitored by ^{31}P and ^{1}H NMR spectroscopy. Complete conversion required ca. 7 days. When CD$_2$Cl$_2$ solutions of *sym*-[**1**(CO)](BF$_4$)$_2$ were stored in the dark, no isomerization was observed, even after several days. When CD$_2$Cl$_2$ solutions of *sym*-[**1**(CO)](BF$_4$)$_2$ were exposed to ambient fluorescent lighting under 1 atm of CO, isomerization slowed and decomposition products were observed by ^{31}P NMR spectroscopy.

Conversion of unsym-[1(CO)]$^{2+}$ to unsym-[1(NCMe)]$^{2+}$. A J-Young tube was charged with 0.005 g (0.004 mmol) of *unsym*-[**1**(CO)]$^{2+}$, and 1 mL of CD$_2$Cl$_2$ was distilled into the J-Young tube at 78 K. The reaction mixture was allowed to warm to room temperature to allow *unsym*-[**1**(CO)]$^{2+}$ to dissolve. The J-Young tube was cooled again to 78 K, and then 0.1 mL of MeCN-d_3 was distilled onto the reaction mixture. The reaction mixture was allowed to warm to room temperature after 30 min (ambient fluorescent lighting). The ^{31}P NMR (CD$_2$Cl$_2$) spectrum was then recorded, which established the presence of unreacted *unsym*-[**1**(CO)]$^{2+}$ (δ 91.4, 72.8, 69.9, 67.6) and *unsym*-[**1**(NCMe)]$^{2+}$ (δ 95.7 (s), 73.6 (t, J_{P-P} = 5 Hz), 70.9 (d, J_{P-P} = 5 Hz), 69.0 (s)). The conversion of *unsym*-[**1**(CO)]$^{2+}$ to *unsym*-[**1**(NCMe)]$^{2+}$ was unaffected by room (fluorescent) light.

Conversion of sym-[1(CO)]$^{2+}$ to unsym-[1(NCMe)]$^{2+}$. A J-Young tube was charged with 0.005 g (0.004 mmol) of *sym*-[**1**(CO)]$^{2+}$, and 1 mL of CD$_2$Cl$_2$ was distilled into the J-Young tube at 78 K. The reaction mixture was allowed to warm to room temperature to allow *sym*-[**1**(CO)]$^{2+}$ to dissolve. The J-Young tube was cooled to 78 K, and then 0.1 mL of MeCN-d_3 was distilled onto the reaction mixture and the reaction mixture allowed to warm to room temperature. After the mixture was allowed to sit for 24 h under ambient fluorescent lighting, the ^{31}P NMR (CD$_2$Cl$_2$) spectrum revealed the presence of *sym*-[**1**(CO)]$^{2+}$ (singlets at δ 86.2 and 81.1) and *unsym*-[**1**(NCMe)]$^{2+}$ (singlets at δ 95.7 and 69.0, triplets at δ 73.6 and 70.9). After 48 h, the conversion of *sym*-[**1**(CO)]$^{2+}$ to *unsym*-[**1**(NCMe)]$^{2+}$ was complete. When conducted in the dark, the conversion required 96 h.

[Fe$_2$(S$_2$C$_2$H$_4$)(CO)$_2$(dppv)$_2$](BF$_4$)$_2$, [1](BF$_4$)$_2$. A solution of 0.050 g (0.0475 mmol) of Fe$_2$(S$_2$C$_2$H$_4$)(CO)$_2$(dppv)$_2$ in 7 mL of CH$_2$Cl$_2$ at −45 °C was treated with 0.030 g (0.0475 mmol) of [CpFe-(C$_5$H$_4$Ac)]BF$_4$ in 3 mL of CH$_2$Cl$_2$. *In situ* IR analysis showed complete conversion to [**1**]$^+$ ($ν_{CO}$ = 1958, 1880 cm^{-1}). The reaction mixture was then treated with a further 0.030 g (0.0475 mmol) of [CpFe(C$_5$H$_4$Ac)]BF$_4$ dissolved in 3 mL of CH$_2$Cl$_2$. *In situ* IR showed complete conversion ($ν_{CO}$ = 1995, 1990 cm^{-1}; see Figure 1). At −45 °C, a stream of CO gas was introduced to the reaction mixture. The IR spectrum showed the change to *unsym*-[**1**]$^{2+}$ within 10 min ($ν_{CO}$ = 2048, 2024, 1896 cm^{-1}).

Supporting Information Available: Crystallographic data for [Fe$_2$(S$_2$C$_2$H$_4$)(μ-CO)(CO)$_2$(dppv)$_2$]BF$_4$ and [Fe$_2$(S$_2$C$_2$H$_4$)(μ-CO)-(CO)$_2$(dppv)$_2$]PF$_6$, voltammograms, and IR, EPR, and ^{31}P NMR spectra. This material is available free of charge via the Internet at http://pubs.acs.org.

JA7113008